PAPER

Renal-clearable hyaluronic acid functionalized NaGdF₄ nanodots with enhanced tumor accumulation†

Yining Yan,[ab] Lei Ding,[a] Lin Liu,*[a] Murad M. A. Abualrejal,[bc] Hongda Chen [iD] *[bc] and Zhenxin Wang[b]

Integration of high tumor-targeting capacity, controlling *in vivo* transport and low normal tissue retention into one engineered nanoparticle is a critical issue for future clinically translatable anti-cancer nanomedicines. Herein, hyaluronic acid functionalized 3.8 nm NaGdF₄ nanodots (named NaGdF₄ ND@HAs) have been prepared through conjugation of tryptone capped NaGdF₄ nanodots (NaGdF₄ ND@tryptone) with hyaluronic acid (HA, a naturally occurring glycosaminoglycan), which can recognize the overexpressed CD44 on cancer cell membranes. The as-prepared NaGdF₄ ND@HAs have good paramagnetic properties (longitudinal relaxivity (r_1) = 7.57×10^{-3} M S^{-1}) and low cytotoxicity. The in vivo experimental results demonstrate that the NaGdF₄ ND@HAs can not only efficiently accumulate in mouse-bearing MDA-MB-231 tumors (*ca.* 5.3% injection dosage (ID) g^{-1} at 2 h post-injection), but also have an excellent renal clearance efficiency (*ca.* 75% injection dosage (ID) at 24 h post-injection). The as-prepared NaGdF₄ ND@HAs have good paramagnetic properties with enhanced tumor-targeting capacity, which provides a useful strategy for the preparation of renal clearable magnetic resonance imaging (MRI) contrast agents for tumors.

Introduction

As one of the prospective directions of contemporary medical sciences, nanomaterial-based theranostics (known as nanomedicines) have been intensively studied because of their potential applications in various domains including diagnosis of and therapies for diseases (*e.g.*, tumor), tracking the location of biomarkers/signal molecules *in vivo*, and evaluating their therapeutic effect.[1–10] To date, more than one hundred nanomedicines have been approved by the Food and Drug Administration (FDA) in the USA, or are in the FDA clinical trial stage.[4] However, it is a great challenge to translate nanomedicines from pre-clinical proof-of-concept to clinical applications because there is an increasing consideration of the biosafety of nanomedicines.[11–18] Currently, many promising nanomedicines normally eliminated through the hepatobiliary route are constructed from relatively large sized (>10 nm in diameter) and nonbiodegradable inorganic nanoparticles.[16–19] However, the

interactions of nanomedicines with mononuclear phagocyte system (MPS) cells (*e.g.*, Kupffer cells) in spleen and liver significantly increase their retention time *in vivo* (even more than months), which causes potential toxicity.[11–19] The biosafety concern can be addressed by the development of nanomedicines that undergo renal clearance.[20–22] During the last few years, several ultra-small sized inorganic nanoparticles (<5.5 nm) have been employed to generate renal clearable nanomedicines for the diagnoses and therapies of various diseases including cancers.[23–33] For instance, Zheng's group has been developed a series of gold nanoparticles/nanoclusters for delivering anticancer drugs,[30] evaluating kidney function,[31] and imaging tumors.[32,33]

As a powerful tool, magnetic resonance imaging (MRI) has been extensively applied for non-invasive diagnoses of various diseases through producing excellent soft-tissue contrast. Compared with other modalities of medical imaging, the sensitivity of MRI is poor. Because trivalent gadolinium ion (Gd^{3+}) has seven unpaired electrons with a large magnetic moment, Gd-chelates and Gd nanoparticles have been employed as contrast agents for enhancing the sensitivity of T_1-weighted MRI.[34–38] Among Gd-based T_1-weighted MRI contrast agents, ultrasmall Gd nanoparticles (also known as Gd nanodots (Gd NDs)) not only have high contrast enhancement capability, but also can be eliminated from body through renal clearance.[39–47] The Gd NDs are normally coated hydrophilic or amphiphilic ligands for improving their colloidal stability and

aDepartment of Radiology, China-Japan Union Hospital of Jilin University, Xiantai Street, Changchun, 130033, P. R. China. E-mail: LiuLin99@jlu.edu.cn

bState Key Laboratory of Electroanalytical Chemistry, Changchun Institute of Applied Chemistry, Chinese Academy of Sciences, Changchun, 130022, P. R. China. E-mail: chenhongda@ciac.ac.cn

cSchool of Applied Chemical Engineering, University of Science and Technology of China, Road Baohe District, Hefei, Anhui, 230026, P. R. China

† Electronic supplementary information (ESI) available. See DOI: 10.1039/c9ra08974h

biocompatibility, then further modified with specific biomolecules for generating high tumor-targeting ability. As a major component of extracellular matrices, hyaluronic acid (hyaluronan, HA) has high binding affinity with cell surface receptor, CD44.[48–50] Therefore, HA can be used as an active tumor-targeting ligand for constructing drug delivery systems since tumor cells normally express high level of CD44.[50–54] For example, Parayath and coauthors have fabricated hyaluronic acid–poly(ethylenimine) (HA–PEI)-based nanoparticles encapsulating miR-125b for anticancer immunotherapy through the interactions of HA with CD44.[53] In addition, Guo *et al.* have found that Gd^{3+}-labeled peptide dendron-HA conjugate-based hybrid (dendronized-HA-DOTA-Gd) has better biocompatibility and higher accumulation in tumors than those of Gd-DTPA.[51] The results suggest that HA might be employed as an active tumor-targeting ligand for generating renal clearable Gd NDs.

In this study, a highly renal-clearable HA functionalized $NaGdF_4$ nanodots ($NaGdF_4$ ND@HAs) were synthesized by a two-step reaction, and evaluated as an active tumor-targeting MRI contrast agent. The tryptone was employed as phase transfer agent for transferring hydrophobic oleic acid coated $NaGdF_4$ nanodots ($NaGdF_4$ ND@OAs, 3.8 nm in diameter) through the Gd–phosphate coordination reaction. HA was then conjugated with the tryptone coated $NaGdF_4$ NDs ($NaGdF_4$ ND@tryptone) by the use of 1-ethyl-3-(3-dimethylaminopropyl) carbodiimide (EDC) as coupling agent. Both *in vitro* cellular studies and *in vivo* small animal experiments of mouse-bearing MDA-MB-231 breast cancer model demonstrated that $NaGdF_4$ ND@HAs exhibit low toxicity and can be used for specific detection of tumors with abundant HA receptor.

Experimental section

Materials

Tryptone was purchased from Oxoid Ltd (Hampshire, England). Oleic acid (OA, 90%), 1-octadecene (ODE, 90%) were obtained from Sigma-Aldrich Co. (St. Louis, USA). The $GdCl_3 \cdot 6H_2O$ was purchased from Beijing HWRK Chem Co. Ltd (Beijing, China). The culture medium Leibovitz L-15 and DMEM were purchased from Jiangsu KeyGen Biotech Co. Ltd (Jiangsu, China). The fetal bovine serum (FBS) was obtained from Gibco Co. (New York, USA). Trypsin–EDTA digest and 3-(4,5-dimethyl-2-thiazolyl)-2,5-diphenyl-2-*H*-tetrazolium bromide (MTT) were purchased from Beijing Dingguo Biotechnology Ltd (Beijing, China). Hyaluronic acid (HA, 4.2 kDa) was purchased from Bloomage Freda Biopharma Co., Ltd (Jinan, China). Other reagents (analytical grade) were purchased from Beijing Chemical Reagent Co. (Beijing, China), which were used without any purification. Deionized H_2O (18.2 MΩ cm) were used in all experiments. All animal procedures were carried out with the procedures approved by the local Animal Research Committee at Jilin University (ethical approve document number: 2019515). Female Balb/c nude mice and Balb/c mice (*ca.*, average body weight of 20 g) were purchased from Liaoning Changsheng Biotechnology Ltd (Liaoning, China). The mice having free access to food and water were kept for 12 h in light and 12 h in dawn daily at 20 °C.

Characterizations

TEM micrographs were recorded by TECNAI G2 high-resolution TEM (FEI Co., USA). Dynamic light scattering and zeta potential of the as-prepared samples were carried out on a Zetasizer Nano ZS (Malvern Instruments Ltd, UK). The analysis of elements was conducted with an ELAN 9000/DRC ICP-MS system (PerkinElmer, USA). The relaxation times of the samples were carried out on a Siemens Prisma 3.0 T MR scanner (Erlangen, Germany). Energy-dispersive X-ray spectra (EDS) were inspected on an energy dispersive spectroscopy (FEI Co., USA). X-ray diffraction analysis were carried out on a D8 ADVANCE diffractometer (Bruker Co., Germany) using Cu Kα (0.15406 nm) radiation. The infrared spectra were conducted with a Vertex 70 Fourier transform infrared (FTIR) spectrometer (Bruker, Germany). XPS measurements were conducted with a VG ESCALAB MKII X-ray photoelectron spectrometer (VG Scientific Ltd, UK) spectroscopy (XPS). Siemens Prisma 3.0 T MR scanner (Erlangen, Germany) was employed to acquire T_1-weighted MR images.

Synthesis of NaGdF₄ ND@HAs

The $NaGdF_4$ ND@OAs were synthesized by previously reported methods (see ESI† for details).[40,43,47] Subsequently, 10 mL $NaGdF_4$ ND@OA cyclohexane solution (1 mg mL^{-1}) were mixed with 10 mL tryptone aqueous solution (6.4 mg mL^{-1}) under vigorously stirred, and incubated at room temperature for 12 h. Then, the as-prepared tryptone capped $NaGdF_4$ nanodots ($NaGdF_4$ ND@tryptone) were purified by centrifugation (13 000 rpm, 3 times) and redispersed in H_2O. 0.5 mL 1-ethyl-3-(3-(dimethylaminopropyl)carbodiimide solution (EDC, 4 mg mL^{-1} in MES (2-(*N*-morpholino)ethanesulfonic acid) buffer) and 0.5 mL *N*-hydroxysulfo-succinimide solution (sulfo-NHS, 6 mg mL^{-1} in MES buffer) were mixed with 2 mL HA solution (2.5 mg mL^{-1} in MES buffer). After incubation at room temperature for 1 h, 2 mL $NaGdF_4$ ND@tryptone (2.5 mg mL^{-1}) in PBS (phosphate buffer saline, pH 7.4)) were added into the mixture and continuously incubated at 37 °C for 3 h. Finally, the as-prepared $NaGdF_4$ ND@HAs were purified by centrifugation (10 000 rpm, 3 times) and redispersed in PBS (pH 7.4).

Cytotoxicity study

The MDA-MB-231 breast cancer cells, MCF-7 breast cancer cells and normal kidney tissue cells (293 cells) were obtained from Shanghai Cell Bank, CAS (Shanghai, China). MDA-MB-231 breast cancer cells were cultured with fresh L-15 culture medium supplemented with 10% FBS in a 96 well plate (1×10^4 cells in 100 μL per well) under full air conditions at 37 °C for 24 h, MCF-7 breast cancer cells and normal kidney tissue cells (293 cells) were cultured with fresh DMEM culture medium supplemented with 10% FBS and 100 U mL^{-1} penicillium–streptomycin in a 96 well plate (1×10^4 cells in 100 μL per well) under 5% CO_2 air conditions at 37 °C for 24 h. Subsequently, those cells were washed by PBS. Next, 100 μL fresh culture medium containing various concentrations (6.25, 12.5, 25, 50, 100 and 200 μg mL^{-1}) of $NaGdF_4$ ND@tryptone or $NaGdF_4$ ND@HAs were introduced into wells, and cultured for another

24 h. After fully washed by PBS (100 μL, 3 times), the cell viabilities were detected by traditional MTT (3-(4,5-dimethyl-2-thiazolyl)-2,5-diphenyl-2-*H*-tetrazolium bromide) assay.

In vitro MRI study

The MDA-MB-231 and MCF-7 cells were cultured at 37 °C for 24 h and divided into 4 groups ((1) MCF-7 + NaGdF$_4$ ND@HAs; (2) free HAs (2 mg mL^{-1}) + MDA-MB-231 incubated for 4 h, and then incubated with NaGdF$_4$ ND@HAs; (3) MDA-MB-231 + NaGdF$_4$ ND@tryptone; (4) MDA-MB-231 + NaGdF$_4$ ND@HAs), which were co-cultured with different concentrations of NaGdF$_4$ ND@tryptone or NaGdF$_4$ ND@HAs in 2 mL fresh culture medium containing different concentrations of NaGdF$_4$ NDs at 37 °C for 24 h, respectively. After washed with fresh culture medium (1 mL, 3 times) and PBS (1 mL, 3 times), the NaGdF$_4$ ND stained cells were digested by 1 mL trypsin and centrifuged at 2000 rpm for 5 min. Subsequently, the as-obtained cell pellets were fixed by 1% agarose gel, and imaged by a Siemens 1.5 T MRI scanner with imaging parameters: 1.2 mm slice thickness, 15 ms echo time (TE), 358 ms repetition time (TR) and 50 mm × 50 mm field of view. In addition, 3×10^3 NaGdF$_4$ ND stained cells were treated by 2 mL aqua regia. The amounts of Gd element in the NaGdF$_4$ ND stained cells were measured by inductively coupled plasma mass spectrometry (ICP-MS, ELAN 9000/DRC, PerkinElmer Co., USA), respectively.

In vivo MRI study

Female Balb/c nude mice and Balb/c mice with average body weight of 20 g were purchased from Liaoning Changsheng Biotechnology Ltd (Liaoning, China). The mice having free access to food and water were kept for 12 h in light/12 h in dawn daily at 20 °C. All animal procedures were approved by the Local Ethics Committee for Institutional Animal Care and Use of Jilin University. MDA-MB-231 cells (1×10^6 cells in 100 μL PBS) were subcutaneously injected into the hind flank of female Balb/c nude mouse. The volume of tumor (V) was evaluated by the following formula: $V = \text{length} \times (\text{width})^2/2$. When V reached about 60 mm^3, the MDA-MB-231 tumor-bearing nude mice were injected intravenously with 100 μL 0.9 wt% NaCl solution containing 2 mg mL^{-1} (Gd^{3+} content) NaGdF$_4$ ND@tryptone or NaGdF$_4$ ND@HAs through tail veins. The *in vivo* MR images of tumors were taken at 0, 0.5, 2, 4, 8, 12, and 24 h post-injection by Siemens 3.0 T MRI scanner with the following scanning parameters: 1.2 mm slice thickness, 3000 ms TR, 9.1 ms TE and 120 mm × 72 mm field of view. In addition, the mice were sacrificed at 2 h post-injection, and the main organs as well as tumors were collected for ICP-MS measurement.

### Biocompatibility analysis

The healthy female Balb/c mice were randomly divided into 2 groups: control group and NaGdF$_4$ ND@HAs treated group. The mice in treated group were injected intravenously with 100 μL 0.9 wt% NaCl solution containing 10 mg kg^{-1} (Gd^{3+} content) NaGdF$_4$ ND@HAs, respectively. The mice in control group were only injected intravenously with 100 μL 0.9 wt% NaCl solution respectively. The body weights of mice were measured every 2

days until 30 days after injection. The mice were sacrificed at the 1st and the 30th day post-injection, and main organs including heart, liver, spleen, lung and kidneys were fixed in 4% (w/v) paraformaldehyde solution, embedded in paraffin, sectioned, and finally stained with hematoxylin–eosin (H&E). Meanwhile, the tumors were fixed in 4% (w/v) paraformaldehyde solution, embedded in paraffin, sectioned, and finally stained by hematoxylin–eosin (H&E) and anti-CD44v6 immunohistochemistry. The blood samples of mice were collected at the 1st and the 30th day post-injection, also analysed by the blood routine assay.

Results and discussion

Synthesis and characterization of NaGdF$_4$ ND@HAs

The synthetic route and application of NaGdF$_4$ ND@HAs is shown in Scheme 1. The hydrophobic NaGdF$_4$ ND@OAs (3.8 ± 0.4 nm in diameter) were prepared by previously reported procedure with a slight modification (as shown in Fig. 1a).[40,43,47] As the digestion product of casein, tryptone contains *ca.* 10–20% casein phosphopeptide (CPP) with the sequence –Ser(P)–Ser(P)–Ser(P)–Glu–Glu–, which can form robust Gd^{3+}–phosphate coordination bonds under mild conditions through the reaction of phosphoseryl serine residue (Ser(P)) and trivalent Gd ions.[43,47] After mixing NaGdF$_4$ ND@OAs with tryptone, hydrophilic NaGdF$_4$ ND@tryptone were generated through replacing the original OA ligand of NaGdF$_4$ ND@OAs by tryptone. Subsequently, HA was activated by EDC and sulfo-NHS, also conjugated on NaGdF$_4$ ND@tryptone surface through the amidation reaction between carboxy group of HA and amine group of tryptone. HA and tryptone, which have been extensively used for producing drugs and health care products, are raw materials approved by the US Food and Drug Administration (FDA). Therefore, the toxicity of NaGdF$_4$ ND can be reduced by HA and tryptone coating. After ligand exchange and HA functionalization, the morphology, size and crystalline nature of NaGdF$_4$ NDs exhibit negligible changes (as shown in Fig. 1b and c). The hydrodynamic diameter and zeta potential of NaGdF$_4$ ND@tryptone were 11.99 nm and −5.86 mV, respectively. The result was consistent with the structure of NaGdF$_4$ ND@tryptone which contains individual solid NaGdF$_4$ ND core and a flexible phosphopeptide outlayer. The phenomenon
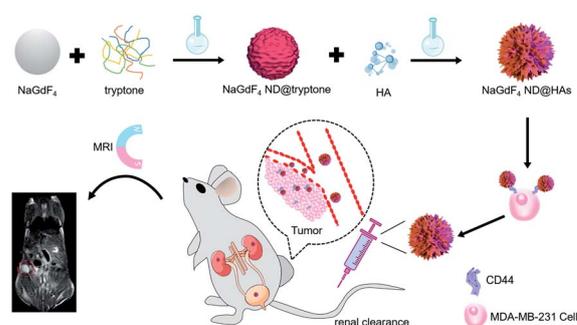
Scheme 1 Schematic diagram of NaGdF4 ND@HAs synthesis, and the application in MRI of tumor through recognizing the overexpressed CD44 on cancer cell membrane.
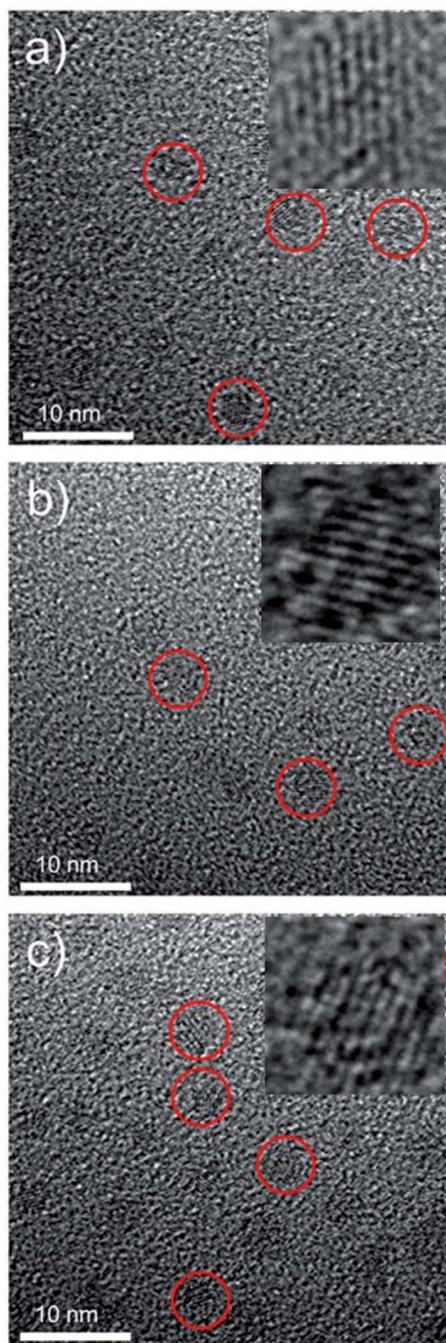
Fig. 1 Transmission electron microscope micrographs (TEM) of (a) $NaGdF_4$ ND@OAs, (b) $NaGdF_4$ ND@tryptone and (c) $NaGdF_4$ ND@HAs, respectively. Insets are corresponding HRTEM micrographs of $NaGdF_4$.

suggested that $NaGdF_4$ ND@tryptone exhibits good monodispersity and negative surface charge. Because HA is negatively charged biomacromolecule, the hydrodynamic diameter of $NaGdF_4$ ND@HAs was increased to 29.05 nm, while the zeta potential of $NaGdF_4$ ND@HAs was deceased to −12.16 mV. The negative surface charge helps to reduce the nonspecific interactions of $NaGdF_4$ NDs with cells. The successful preparation of $NaGdF_4$ ND@tryptone and $NaGdF_4$ ND@HAs were also

investigated by XPS, EDS and FTIR. After incubation with tryptone, the phosphorus and nitrogen peaks were clearly observed in the XPS (P 2p (133 eV) and N 1s (400 eV)) and EDS (P (2.01 keV) and N (0.39 keV)) spectra of $NaGdF_4$ NDs (as shown in Fig. S1 and S2†).[43,47,55] In addition, the XPS spectrum of $NaGdF_4$ ND@HAs exhibited relatively high intensity of C 1s (284 eV). Compared to $NaGdF_4$ ND@OAs, two additional IR bands at 683 cm^{-1} and 1080 cm^{-1} are observed in FTIR spectrum of $NaGdF_4$ ND@tryptone (as shown in Fig. S3†), which are corresponded to the out-of-plane bending vibration of C–H bond on benzene ring and antisymmetric bending mode of PO_4^{3-}, respectively.[56] A new IR band at 1010 cm^{-1} is observed in FTIR spectrum of $NaGdF_4$ ND@HAs (as shown in Fig. S3†), which is corresponded to stretching vibration of C–O band of primary alcohol of HA.[57] As shown in Fig. 2, the longitudinal relaxivity (r_1) value (7.57 mM^{-1} S^{-1}) of $NaGdF_4$ ND@HAs is higher than those of $NaGdF_4$ ND@tryptone (6.03 mM^{-1} S^{-1}) as well as commercial Gd^{3+} chelates (e.g., (4.3 mM^{-1} S^{-1})). The high r_1 value of $NaGdF_4$ ND@HAs may stem from the strong polarity of HA molecule which may cause a spatial agglomeration of water around the Gd^{3+}, leading to boost the relaxivity to high value. The result indicates that $NaGdF_4$ ND@HAs can be used as efficient T_1-weighted MRI contrast agent.

The interactions of $NaGdF_4$ ND with living cells

Human triple-negative breast carcinoma MDA-MB-231 cell line was selected as a typical model because it expresses high level of CD44.[58] As shown in Fig. S4,† the MDA-MB-231, MCF-7 and 293 cells exhibit higher than 90% viability after incubated with up to 200 µg mL^{-1} $NaGdF_4$ ND@HAs or $NaGdF_4$ ND@tryptone for 24 h. The result indicates that both of $NaGdF_4$ ND@HAs and $NaGdF_4$ ND@tryptone have low cytotoxicity. The T_1-weighted MR signal intensity of $NaGdF_4$ ND@HAs stained MDA-MB-231 cells was stronger than which of $NaGdF_4$ ND@tryptone stained MDA-MB-231 cells or $NaGdF_4$ ND@HAs stained MCF-7 (as shown in Fig. 3a–c). The T_1-weighted MR signal intensity
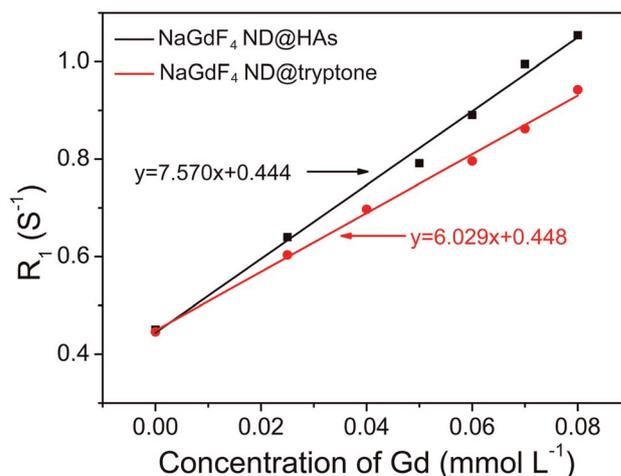

Fig. 2 R_1 relaxivities of $NaGdF_4$ ND@tryptone and $NaGdF_4$ ND@HAs as a function of the molar concentration of Gd^{3+} in solution, respectively. The slope of line represents the longitudinal relaxivity (r_1) value.
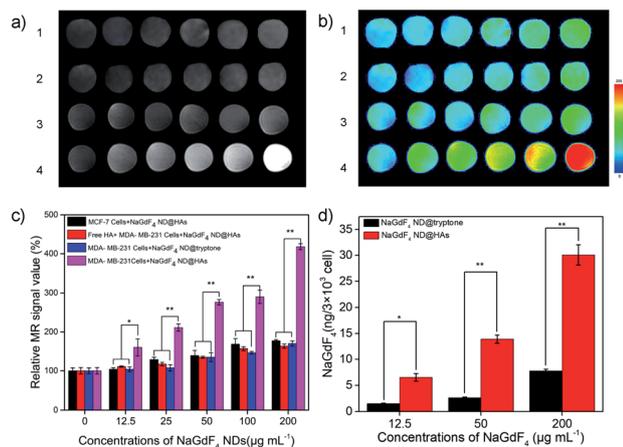
Fig. 3 (a) MR images of $NaGdF_4$ ND stained cells. ((1) MCF-7 cells + $NaGdF_4$ ND@HAs; (2) free HA + MDA-MB-231 cells + $NaGdF_4$ ND@HAs; (3) MDA-MB-231 cells + $NaGdF_4$ ND@tryptone; (4) MDA-MB-231 cells + $NaGdF_4$ ND@HA), (b) corresponding pseudo-color images and (c) corresponding data analysis of $NaGdF_4$ ND stained cells. The cells were incubated with 0, 12.5, 25, 50, 100, 200 μg mL^{-1} $NaGdF_4$ ND@tryptone or $NaGdF_4$ ND@HAs from left to right, respectively. (d) The amounts of Gd element in the $NaGdF_4$ ND stained cells. Error bars mean standard deviations ($n = 5$, $*P < 0.05$ or $**P < 0.01$ from an analysis of variance with Tukey's post-test).

(Fig. 3, group 2) of NaGdF4 ND@HAs stained HA treated MDA-MB-231 cells is much lower than which of NaGdF4 ND@HAs stained untreated MDA-MB-231 cells (Fig. 3, group 4). In addition, the cellular internalization amount of $NaGdF_4$ ND@HAs is much higher than which of $NaGdF_4$ ND@tryptone (as shown in Fig. 3d). The results demonstrate that the $NaGdF_4$ ND@HAs have high affinity with MDA-MB-231 cells, and can be used to recognize CD44-overexpression cells with high specificity.

In vivo MRI of MDA-MB-231 tumor

A Balb/c nude mouse bearing MDA-MB-231 tumor model was established for evaluating the active tumor-targeting capacity of $NaGdF_4$ ND@HAs. Both of $NaGdF_4$ ND@HAs and $NaGdF_4$ ND@tryptone (10 mg Gd kg^{-1} body weight in 0.9 wt% NaCl) were intravenously injected into the mouse bearing MDA-MB-231 tumor through tail vein and the MR signals of tumor sites were recorded at desired timed intervals within 24 h post-injection. The $NaGdF_4$ ND@tryptone can be accumulated in tumor site through enhanced permeability and retention (EPR) effect (*i.e.*, passive tumor-targeting), while $NaGdF_4$ ND@HAs can be accumulated in tumor site by EPR effect and binding of HA with CD44 (*i.e.*, active tumor-targeting). As expected, the MR signals of the tumor sites gradually increased by numbers in between 0 and 2 h post-injection (as shown in Fig. 4). Maximum MR contrast enhancement is obtained at 2 h post-injection of $NaGdF_4$ NDs. In particular, the MR signal intensity in tumor site of $NaGdF_4$ ND@HAs treated mouse is higher than which of $NaGdF_4$ ND@tryptone treated mouse at the same post-injection time point. The maximum MR contrast enhancement in tumor site of $NaGdF_4$ ND@HAs treated mouse is 1.6 times higher than which of the $NaGdF_4$ ND@tryptone treated mouse. The

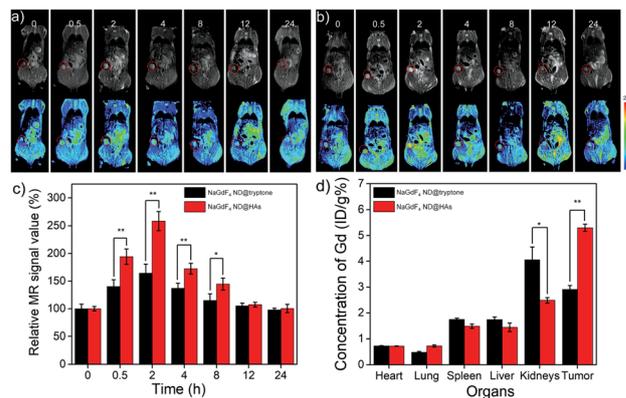**Fig. 4** *In vivo* MR images and corresponding pseudo color images of Balb/c mouse bearing MDA-MB-231 tumor after intravenous injection of (a) $NaGdF_4$ ND@tryptone or (b) $NaGdF_4$ ND@HAs (10 mg Gd kg^{-1} body) at different timed intervals (0 (pre-injection), 0.5, 2, 4, 8, 12 and 24 h post-injection), respectively. (c) Corresponding data analysis of MR measurements. The tumor site was marked by circle. (d) The amounts of $NaGdF_4$ NDs in main organs at 2 h post-injection. Error bars mean standard deviations ($n = 5$, $*P < 0.05$ or $**P < 0.01$ from an analysis of variance with Tukey's post-test).

phenomenon may due to high binding affinity of HA with over expressed CD44 on MDA-MB-231 cells. The result demonstrated that the as-prepared $NaGdF_4$ ND@HAs can be severed as an excellent T_1-weighted MRI contrast agent for detection of CD44-overexpression tumors (*e.g.*, triple-negative breast cancer). The active tumor-targeting capacity of $NaGdF_4$ ND@HAs was also confirmed by ICP-MS measurement. As shown in Fig. 4d, the amounts of Gd in kidneys and tumors were relatively higher than in other organs, indicating that both $NaGdF_4$ ND@tryptone and $NaGdF_4$ ND@HAs can be efficiently accumulated in tumor sites and excreted by renal clearance. In particular, the Gd content in tumor of $NaGdF_4$ ND@HAs treated mouse treated mouse was 1.87 times higher than which of $NaGdF_4$ ND@tryptone treated mouse. The result indicated that the accumulation amount of $NaGdF_4$ ND@HAs in tumor site is clearly improved through EPR effect as well as recognition of HA receptors of tumor cells.

In vivo biodistribution and toxicology of $NaGdF_4$ ND@HAs

For evaluating its biodistribution and clearance pathway, $NaGdF_4$ ND@HAs (10 mg Gd kg^{-1} body weight in 0.9 wt% NaCl) were injected into healthy Balb/c mice through tail vein. The MR signals in the liver, kidneys and bladder were recorded at different timed intervals of post-injection (as shown in Fig. 5a and S5†). The MR signal of liver exhibited little change during the whole period, indicating low accumulation of $NaGdF_4$ ND@HAs in liver. MR signals in the kidneys and bladder were clearly enhanced within 24 h post-injection, and recovered to pre-injection levels after 24 h post-injection. The result demonstrated that $NaGdF_4$ ND@HAs are excreted from the body by renal clearance. After intravenous injection of $NaGdF_4$ ND@HAs, the Gd content in urine of mouse was measured for addressing the pharmacokinetics behavior of $NaGdF_4$ ND@HAs
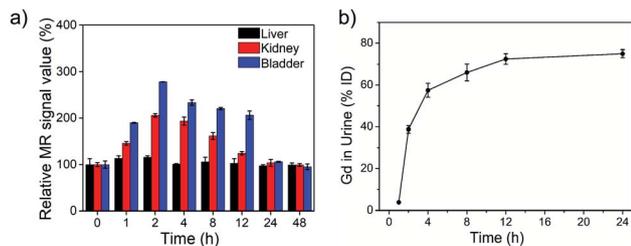
Fig. 5 (a) The MR signal intensities of liver, kidney and bladder of healthy Balb/c mice after intravenous injection of NaGdF$_4$ ND@HAs at different time intervals (0 (pre-injection), 1, 2, 4, 8, 12, 24 and 48 h) of post-injection, respectively. (b) The total amounts of NaGdF$_4$ ND@HAs in mouse urine as a function of post-injection times. Error bars mean standard deviations ($n = 5$).

(as shown in Fig. 5b). The total of Gd element in urine of NaGdF$_4$ ND@HAs treated mouse increased significantly from 0 to 12 h post-injection. About 75% Gd was found in urine after 24 h administration, confirming that NaGdF$_4$ ND@HAs were efficiently excreted with the urine. In addition, the NaGdF$_4$ ND@HAs showed a negligible morphology change after *in vivo* circulation, which indicated that the NaGdF$_4$ ND@HAs have good colloidal stability *in vivo* (as shown in Fig. S6†). The efficient renal clearance of NaGdF$_4$ ND@HAs helped to eliminate potential hazards of long-term *in vivo* toxicity.

For further evaluating the biocompatibility, the healthy Balb/c mice were intravenously injected at a single dose of NaGdF$_4$ ND@HAs (10 mg Gd kg^{-1} body weight in 0.9 wt% NaCl). The bodyweights of NaGdF$_4$ ND@HAs treated mice increased steadily as the time prolonged, which was consistent with those of control group (as shown in Fig. S7†). The result suggested that NaGdF$_4$ ND@HAs have little effect on the growth and development of mice. The main organs (heart, liver, spleen, lung and kidneys) were collected for histology analysis at the 1st day and the 30th day post-injection. Comparing with the control group, the main organs of NaGdF$_4$ ND@HAs treated mice showed negligible lesions or abnormalities (as shown in Fig. 6). Tumor tissue from the mice were collected for H&E staining and anti-CD44v6 staining, respectively. The experimental result indicated that cel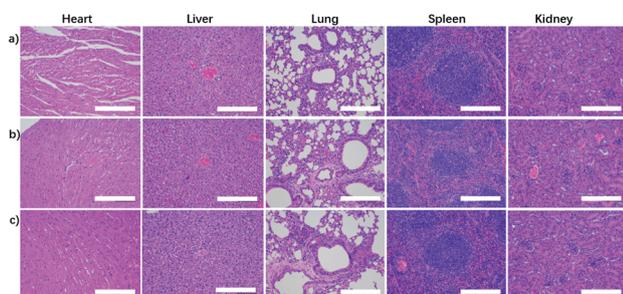l membrane surface receptor CD44 was overexpressed on the tumor tissue (as shown in Fig. S8†). Hematology analysis was carried out for monitoring acute and long-term toxicity of NaGdF$_4$ ND@HAs at the 1st day and the 30th day post-injection, respectively. There was little difference between NaGdF$_4$ ND@HAs treated group and control group (as shown in Table S1†). These results demonstrated that NaGdF$_4$ ND@HAs have good biocompatibilities.

Conclusions

In summary, the renal clearable NaGdF$_4$ ND@HAs have been prepared by a two-step reaction through strong interaction of Gd^{3+} with phosphonate groups in tryptone and amidation reaction between carboxy group of HA and amine group of tryptone. *In vitro* and *in vivo* experimental results demonstrate that the as-prepared NaGdF$_4$ ND@HAs display high MDA-MB-231 tumor-targeting capacity. The NaGdF$_4$ ND@HAs have held great potential as an excellent MR contrast agent for detection CD44-overexpression tumor since advantages of NaGdF$_4$ ND@HAs including high tumor targeting ability, efficient renal clearance capacity and excellent biocompatibility satisfied the basic standards of clinical applications.

Conflicts of interest

There are no conflicts to declare.

Acknowledgements

References

1 D. Peer, J. M. Karp, S. Hong, O. C. Farokhzad, R. Margalit and R. Langer, *Nat. Nanotechnol.*, 2007, **2**, 751–760.
2 E. C. Dreaden, A. M. Alkilany, X. Huang, C. J. Murphy and M. A. El-Sayed, *Chem. Soc. Rev.*, 2012, **41**, 2740–2779.
3 G. Chen, I. Roy, C. Yang and P. N. Prasad, *Chem. Rev.*, 2016, **116**, 2826–2885.
4 D. Bobo, K. J. Robinson, J. Islam, K. J. Thurecht and S. R. CCorrie, *Pharm. Res.*, 2016, **33**, 2373–2387.
5 X. Huang, Y. Liu, B. Yung, Y. Xiong and X. Chen, *ACS Nano*, 2017, **11**, 5238–5292.
6 Z. Liu, W. Jiang, J. Nam, J. J. Moon and B. Y. S. Kim, *Nano Lett.*, 2018, **18**, 6655–6659.
7 C. M. Hartshorn, M. S. Bradbury, G. M. Lanza, A. E. Nel, J. Rao, A. Z. Wang, U. B. Wiesner, L. Yang and P. Grodzinski, *ACS Nano*, 2018, **12**, 24–43.
8 M. Overchuk and G. Zheng, *Biomaterials*, 2018, **156**, 217–237.
9 J. Gupta, M. T. Fatima, Z. Islam, R. H. Khan, V. N. Uversky and P. Salahuddin, *Int. J. Biol. Macromol.*, 2019, **130**, 515–526.
10 Y. Liu, P. Bhattarai, Z. Dai and X. Chen, *Chem. Soc. Rev.*, 2019, **48**, 2053–2108.
11 E. K. Lim, T. Kim, S. Paik, S. Haam, Y. M. Huh and K. Lee, *Chem. Rev.*, 2015, **115**, 327–394.

Fig. 6 H&E staining revealed tissue sections from the mice with (a) 0.9% NaCl solution (control) and NaGdF$_4$ ND@HAs (10 mg Gd kg^{-1} body) at (b) 1 day and (c) 30 days post-injection respectively. The scale bars are 200 μm.

12 J. I. Hare, T. Lammers, M. B. Ashford, S. Puri, G. Storm and S. T. Barry, *Adv. Drug Delivery Rev.*, 2017, **108**, 25–38.

13 M. M. Alvarez, J. Aizenberg, M. Analoui, A. M. Andrews, G. Bisker, E. S. Boyden, R. D. Kamm, J. M. Karp, D. J. Mooney, R. Oklu, D. Peer, M. Stolzoff, M. S. Strano, G. Trujillo-de Santiago, T. J. Webster, P. S. Weiss and A. Khademhosseini, *ACS Nano*, 2017, **11**, 5195–5214.

14 J. Shi, P. W. Kantoff, R. Wooster and O. C. Farokhzad, *Nat. Rev. Cancer*, 2017, **17**, 20–37.

15 J. Paradise, *AMA J. Ethics*, 2019, **21**(4), E347–E355.

16 R. A. Petros and J. M. DeSimone, *Nat. Rev. Drug Discovery*, 2010, **9**, 615–627.

17 P. Cai, X. Zhang, M. Wang, Y. L. Wu and X. Chen, *ACS Nano*, 2018, **12**, 5078–5084.

18 S. Sharifi, S. Behzadi, S. Laurent, M. Laird Forrest and P. Stroeve, *Chem. Soc. Rev.*, 2012, **41**, 2323–2343.

19 X. Wang, L. Guo, S. Zhang, Y. Chen, Y. T. Chen, B. Zheng, J. Sun, Y. Qian, Y. Chen, B. Yan and W. Lu, *ACS Nano*, 2019, **13**, 5720–5730.

20 E. B. Ehlerding, F. Chen and W. Cai, *Adv. Sci.*, 2016, **3**, 1500223.

21 L. Gong, Y. Wang and J. Liu, *Biomater. Sci.*, 2017, **5**, 1393–1406.

22 B. Du, M. Yu and J. Zheng, *Nat. Rev. Mater.*, 2018, **3**, 358–374.

23 T. Cao, Y. Yang, Y. Sun, Y. Wu, Y. Gao, W. Feng and F. Li, *Biomaterials*, 2013, **34**, 7127–7134.

24 F. Liu, X. He, H. Chen, J. Zhang, H. Zhang and Z. Wang, *Nat. Commun.*, 2015, **6**, 8003.

25 M. Yu, J. Liu, X. Ning and J. Zheng, *Angew. Chem., Int. Ed.*, 2015, **54**, 15654–15658.

26 D. Ni, D. Jiang, H. F. Valdovinos, E. B. Ehlerding, B. Yu, T. E. Barnhart, P. Huang and W. Cai, *Nano Lett.*, 2017, **17**, 3282–3289.

27 Y. Cui, J. Yang, Q. Zhou, P. Liang, Y. Wang, X. Gao and Y. Wang, *ACS Appl. Mater. Interfaces*, 2017, **9**, 5900–5906.

28 Q. Wei, Y. Chen, X. Ma, J. Ji, Y. Qiao, B. Zhou, F. Ma, D. Ling, H. Zhang, M. Tian Mei, J. Tian and Z. Min, *Adv. Funct. Mater.*, 2018, **28**, 1704634.

29 Y. Wang, S. Ma, Z. Dai, Z. Rong and J. Liu, *Nanoscale*, 2019, **11**, 16336–16341.

30 C. Peng, M. Yu, J. T. Hsieh, P. Kapur and J. Zheng, *Angew. Chem.*, 2019, **58**, 12076–12080.

31 M. Yu, J. Zhou, B. Du, X. Ning, C. Authement, L. Gandee, P. Kapur, J.-T. Hsieh and J. Zheng, *Angew. Chem., Int. Ed.*, 2016, **55**, 2787–2791.

32 J. Liu, M. Yu, C. Zhou, S. Yang, X. Ning and J. Zheng, *J. Am. Chem. Soc.*, 2013, **135**, 4978–4981.

33 C. Peng, X. Gao, J. Xu, B. Du, X. Ning, S. Tang, R. M. Bachoo, M. Yu, W. P. Ge and J. Zheng, *Nano Res.*, 2017, **10**, 1366–1376.

34 M. Bottrill, L. Kwok and N. J. Long, *Chem. Soc. Rev.*, 2006, **35**, 557–571.

35 H. B. Na, I. C. Song and T. Hyeon, *Adv. Mater.*, 2009, **21**, 2133–2148.

36 L. Zhang, R. Liu, H. Peng, P. Li, Z. Xu and A. K. Whittaker, *Nanoscale*, 2016, **8**, 10491–10510.

37 Y. Cao, L. Xu, Y. Kuang, D. Xiong and R. Pei, *J. Mater. Chem. B*, 2017, **5**, 3431–3461.

38 L. Zeng, D. Wu, R. Zou, T. Chen, J. Zhang and A. Wu, *Curr. Med. Chem.*, 2018, **25**, 2970–2986.

39 J. Y. Park, M. J. Baek, E. S. Choi, S. Woo, J. H. Kim, T. J. Kim, J. C. Jung, K. S. Chae, Y. Chang and G. H. Lee, *ACS Nano*, 2009, **3**, 3663–3669.

40 N. J. J. Johnson, W. Oakden, G. J. Stanisz, R. S. Prosser and F. C. J. M. van Veggel, *Chem. Mater.*, 2011, **23**, 3714–3722.

41 G. Liang, L. Cao, H. Chen, Z. Zhang, S. Zhang, S. Yu, X. Shen and J. Kong, *J. Mater. Chem. B*, 2013, **1**, 629–638.

42 J. Fang, P. Chandrasekharan, X. L. Liu, Y. Yang, Y. B. Lv, C. T. Yang and J. Ding, *Biomaterials*, 2014, **35**, 1636–1642.

43 F. Liu, X. He, J. Zhang, H. Zhang and Z. Wang, *Small*, 2015, **11**, 3676–3685.

44 X. Jin, F. Fang, J. Liu, C. Jiang, X. Han, Z. Song, J. Chen, G. Sun, H. Lei and L. Lu, *Nanoscale*, 2015, **7**, 15680–15688.

45 K. Ni, Z. Zhao, Z. Zhang, Z. Zhou, L. Yang, L. Wang, H. Ai and J. Gao, *Nanoscale*, 2016, **8**, 3768–3774.

46 X. Zheng, K. Zhao, J. Tang, X. Wang, L. Li, N. Chen, Y. Wang, S. Shi, X. Zhang and S. Malaisamy, *ACS Nano*, 2017, **11**, 3642–3650.

47 H. Chen, X. Li, F. Liu, H. Zhang and Z. Wang, *Mol. Pharmaceutics*, 2017, **14**, 3134–3141.

48 B. P. Toole, *Nat. Rev. Cancer*, 2004, **4**, 528–539.

49 C. Underhill, *J. Cell Sci.*, 1992, **103**, 293–298.

50 J. Lesley, R. Hyman, N. English, J. B. Catterall and G. A. Turne, *Glycoconjugate J.*, 1997, **14**, 611–622.

51 C. Guo, L. Sun, H. Cai, Z. Duan, S. Zhang, Q. Gong, K. Luo and Z. Gu, *ACS Appl. Mater. Interfaces*, 2017, **9**, 23508–23519.

52 G. Huang and H. Huang, *J. Controlled Release*, 2018, **278**, 122–126.

53 N. N. Parayath, A. Parikh and M. M. Amiji, *Nano Lett.*, 2018, **18**, 3571–3579.

54 Y. Cheng, X. Tan, J. Wang, Y. Wang, Y. Song, Q. You, Q. Sun, L. Liu, S. Wang, F. Tan, J. Li and N. Li, *J. Controlled Release*, 2018, **277**, 77–88.

55 Y. Cao, M. L. Mei, J. Xu, E. C. M. Lo, Q. Li and C. H. Chu, *J. Dent.*, 2013, **41**, 818–825.

56 C. Holt, N. M. Wahlgren and T. Drakenberg, *Biochem. J.*, 1996, **314**, 1035–1039.

57 R. Gilli, M. KacurBkova, M. Mathlouthi, L. Navarini and S. Paoletti, *Carbohydr. Res.*, 1994, **263**, 315–326.

58 Y. Fan, Q. Wang, G. Lin, Y. Shi, Z. Gu and T. Ding, *Acta Biomater.*, 2017, **62**, 257–272.